The bound state spectrum of HOBr up to the dissociation limit: Evolution of saddle-node bifurcations

Tarek Azzam and Reinhard Schinke[a)]
Max-Planck-Institut für Strömungsforschung, D-37073 Göttingen, Germany

Stavros C. Farantos
Institute of Electronic Structure and Laser Foundation for Research and Technology-Hellas, Greece, and Department of Chemistry, University of Crete, Iraklion 711 10, Crete, Greece

Marc Joyeux
Laboratoire de Spectrométrie Physique, Université Joseph Fourier-Grenoble I, BP 87, F-38402, St Martin d'Heres Cedex, France

Kirk A. Peterson
Department of Chemistry, Washington State University, Pullman, Washington 99164-4630

(Received 5 November 2002; accepted 5 March 2003)

Based on an accurate potential energy surface [J. Chem. Phys. **113**, 4598 (2000)] we calculated *ca.* 700 bound state energies and wave functions of nonrotating HOBr using the filter-diagonalization method. Similar to HOCl, a 1:2 anharmonic resonance between the HOBr bending and the OBr stretching mode determines the general structure of the level spectrum. One of the results of this resonance is a saddle-node bifurcation at which a new class of states (''dissociation states'') comes into existence, which advance along the HO–Br dissociation path. Because the resonance condition at low energies is better fulfilled for HOBr, the bifurcation occurs at considerably lower energies than for HOCl. The results of the quantum mechanical calculations are interpreted in terms of classical periodic orbits (continuation/bifurcation diagram) and a semiclassical analysis based on a spectroscopic Hamiltonian, which is fitted to the exact energy levels and also taking into account the wave functions. © *2003 American Institute of Physics.* [DOI: 10.1063/1.1569914]

I. INTRODUCTION

In recent years, the vibrational spectra of several triatomic molecules have been investigated in great detail by quantum mechanical, classical, and semiclassical methods.[1] The vibrational energies and wave functions from the bottom of the potential well up to very high energies, in several cases even above the dissociation threshold, have been analyzed. Examples are HCP[2,3] and DCP,[4] HCO[5] and DCO,[6] and HOCl.[7,8] Such systematic studies reveal the evolution of the spectrum with energy and the development of special features like bifurcations, for example. The analysis of the classical phase space in terms of periodic orbits (PO)[9,10] and continuation/bifurcation (C/B) diagrams[11] has been very helpful in understanding the quantum mechanical spectra.[12] In many cases, additional insight has been obtained from the semiclassical investigation of approximate, yet accurate spectroscopic Hamiltonians.[7,13–15] Knowledge of the structure of the spectrum, and especially the shape of the corresponding wave functions, at energies close to the dissociation limit is also important for understanding the lifetime of resonance states in the continuum.[16–19]

The bound-state spectrum of HOCl has been thoroughly studied. Accurate potential energy surfaces (PES) have been constructed[8,20–22] and all bound state energies and wave functions have been calculated and assigned, whenever possible.[7,8] Classical and semiclassical analyses have also been performed.[7,8,23] The key feature of HOCl is a 1:2 Fermi (anharmonic) resonance between the HOCl bending and the OCl stretching coordinate. The resonance is only approximately fulfilled at low energies, but becomes more and more valid with increasing energy. As a consequence, a saddle-node (SN) bifurcation exists at relatively high energies, that is, a new family of quantum mechanical states appears, which does not exist at low energies. The OH stretching mode is only weakly coupled to the other two degrees of freedom.

Hypobromous acid, HOBr, is very similar to HOCl, except that the mass of the dissociating atom, Br, is approximately 2.25 times heavier than Cl. The difference of the reduced mass associated with the dissociation coordinate will lead, together with a slightly different PES, to a variation of the frequency ratios and therefore to a different resonance pattern in the spectrum of vibrational states. Although the HOBr spectrum is very similar to the spectrum of HOCl, there are some interesting changes, which will be highlighted in the present article.

The present study is based on the calculated PES of Peterson.[24] Peterson also calculated the vibrational energies up to the dissociation threshold. However, a detailed analysis, especially of the various bifurcations and the types of wave functions existing in the high-energy regime, has not been undertaken. This is the topic of the present study. The article is organized in the following way: The computational

[a)]Electronic mail: rschink@gwdg.de

details of the quantum mechanical calculations are described in Sec. II. Subsequently, the quantum mechanical spectrum is described in a more phenomenological way in Sec. III and the main observations are explained in terms of the structure of the classical phase space in Sec. IV. The semiclassical analysis of a spectroscopic Hamiltonian fit to the quantum mechanical spectrum provides additional insight and is described in Sec. V. Finally, a brief summary closes this article in Sec. VI.

II. COMPUTATIONAL DETAILS

Except if otherwise noted, energies (in eV) are quoted with respect to the global minimum of the PES. The calculations are similar to those for HOCl[8] and only differ in the parameters of the three-dimensional grid. The usual Jacobi coordinates R, r, and γ appropriate for HO–Br are employed. The bound states are calculated by the filter diagonalization (FD) technique, as developed by Neuhauser, Taylor, and Mandelshtam.[25–27] All in all, a total of 708 bound states has been calculated with 20 energy windows. While the lowest-energy window was chosen to have a width of 1 eV, the highest-energy window covered a region of only 0.02 eV.

The wave functions are represented on a discrete-variable-representation (DVR) grid.[28] For the highest-energy windows the R grid is chosen to extend from $2.5a_0$ to $10.0a_0$ with 225 potential-optimized points.[29] As for HOCl[8] 70 Gauss–Legendre quadrature points[30] are found sufficient for the angular grid, where γ ranges from 0° to 180°. The choice of the r grid is more intricate. An inspection of the minimal energy path of the potential along r reveals a second small potential well that extends from $3.3a_0$ to $7.5a_0$ with a minimum at 2.658 eV (with respect to the HOBr minimum) for $r=4.86a_0$. It corresponds to the HBrO isomer. Test calculations have shown that it is necessary to include this minimum on the grid, especially for the high overtone states of the OH stretching coordinate, and therefore the grid in r is chosen to extend from $1a_0$ to $7.5a_0$ with 74 potential-optimized points. As a consequence, the three-dimensional grid is very large. Apart from the lowest-energy windows, which had a smaller range in R than reported above $(2.5a_0-6a_0)$, there are $N=1\,165\,500$ grid points. Eliminating all points from the grid, which have a potential energy higher than $V_{\mathrm{cut}}=4.4$ eV, reduces the grid to $N=323\,435$. Convergence in the highest-energy window requires 210 000 Chebychev iterations.

The vibrational energies calculated in this study agree very well with those calculated by Peterson using a truncation/recoupling technique.[24] The differences are of the order of only few tenths of a cm^{-1} for the low and the medium energy range and generally of the order of one cm^{-1} for the highest bound states.

III. PHENOMENOLOGICAL DESCRIPTION OF THE QUANTUM MECHANICAL SPECTRUM

The dissociation energy for HOBr is $D_0=17\,210\,\mathrm{cm}^{-1}$ (Ref. 24, Table III), slightly smaller than that for HOCl, which is $D_0=19\,290\,\mathrm{cm}^{-1}$ (Ref. 31). As a consequence, there are—despite the heavier mass of Br—slightly less bound states (708) than for HOCl (827). All of the 708 bound states have been visually inspected and about 650 of them could be reasonably assigned in the same way as thoroughly discussed by Weiß *et al.*[8] for HOCl. A list of all bound states and assignments are published electronically.[32] A few assignments differ from the *ca.* 90 assignments previously given by Peterson.[24] In what follows, v_1, v_2, and v_3 are the HO stretching, the bending, and the OBr stretching quantum numbers, respectively. The OH stretching mode is rather weakly coupled to the other two modes. It is therefore possible to consider the spectra for individual values of v_1 separately. We begin with the spectrum for $v_1=0$ and make a few comments for $v_1\neq 0$ at the end of this section.

A. The bending and the HO–Br stretching progression

The calculated transition energies for the fundamentals are 3615.0, 1162.8, and 620.2 cm^{-1}. Similar to HOCl, the OBr stretching and the bending modes form a 1:2 anharmonic resonance, with twice the stretching frequency being approximately equal to the bending frequency. The mismatch is merely 78 cm^{-1}, as compared to 206 cm^{-1} for HOCl.[8] As a consequence of the resonance, for a given value of v_1 the eigenenergies can be grouped into polyads $[v_1,P]$, with $P=2v_2+v_3$ being the polyad number. Since $2\omega_3$ is greater than ω_2, at low energies the states of the fast mode, γ, are located at the bottom of the polyad and the states of the slow mode, R, are at the top.

Changes in the structure of polyads and the wave functions are caused by the 1:2 anharmonic resonance. At low energies, polyads are compact and well separated. Because of the better fulfillment of the resonance condition for HOBr as compared to HOCl, the energy gap between the lowest and the highest state in a polyad is smaller for HOBr. Nevertheless, with increasing energy the polyads become wider in energy and from $P=19$ onward polyads with $v_1=0$ overlap.

Figure 1, depicting all wave functions of polyad [0,12], illustrates the low-energy behavior of the wave functions. The relatively strong curvature for the wave function of state (0,0,12) clearly manifests the 1:2 resonance. At very low energies, the $(0,0,v_3)$ states more or less are aligned along the dissociation coordinate R. However, due to the resonance with the bending states, they acquire increasingly more bending character and thereby avoid the dissociation path, as already clearly seen in Fig. 1. As a consequence, the frequencies, i.e., the energy differences between neighboring states, for the $(0,v_2,0)$ and $(0,0,v_3)$ progressions become almost identical for $P\approx 7-8$ as seen in Fig. 2(b). Since ω_2 is in closer resonance to $2\omega_3$ for HOBr, the curvature of the $(0,0,v_3)$ wave functions is larger—for the same polyad—for HOBr than for HOCl.

At higher energies there are two additional developments of the bending and stretching progressions worth mentioning. First, starting with $v_2=11$, the pure bending overtone states $(0,v_2,0)$ develop a node along the R coordinate and appear more like $(0,v_2,1)$. One example, (0,12,0), is depicted in Fig. 3(d). In view of the classical periodic orbit analysis in Sect. IV, this behavior is the consequence of a period-doubling (PD) bifurcation for the family of bending

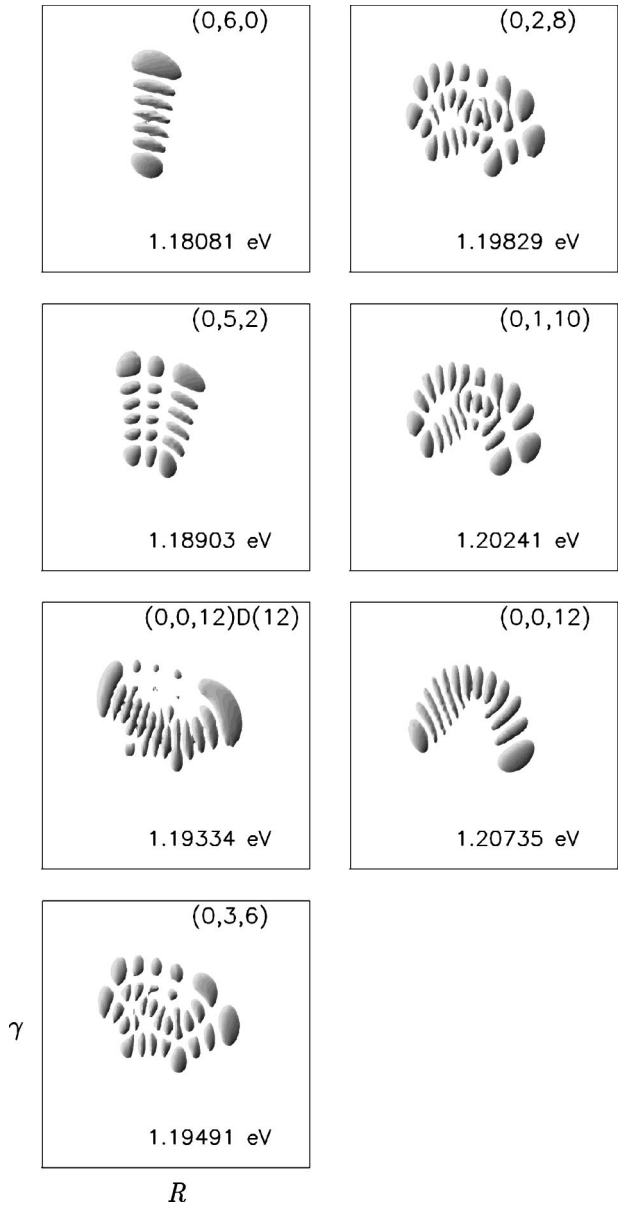

FIG. 1. Wave functions for polyad $P=12$. The γ axis ranges from 0° to 179° and the R axis ranges from $2.5a_0$ to $5a_0$. All wave function plots depicted in this article, if not stated otherwise, have been obtained from a plotting routine, which allows us to rotate 3-D objects in space. Shown is one particular contour $\epsilon(R,r,\gamma)=\sin\gamma|\Psi(R,r,\gamma|^2$, with the value of ϵ being the same in one figure. The plots are viewed along the r axis, in the direction perpendicular to the plane spanned by R and γ. Shading emphasizes the 3-D character of the wave functions.

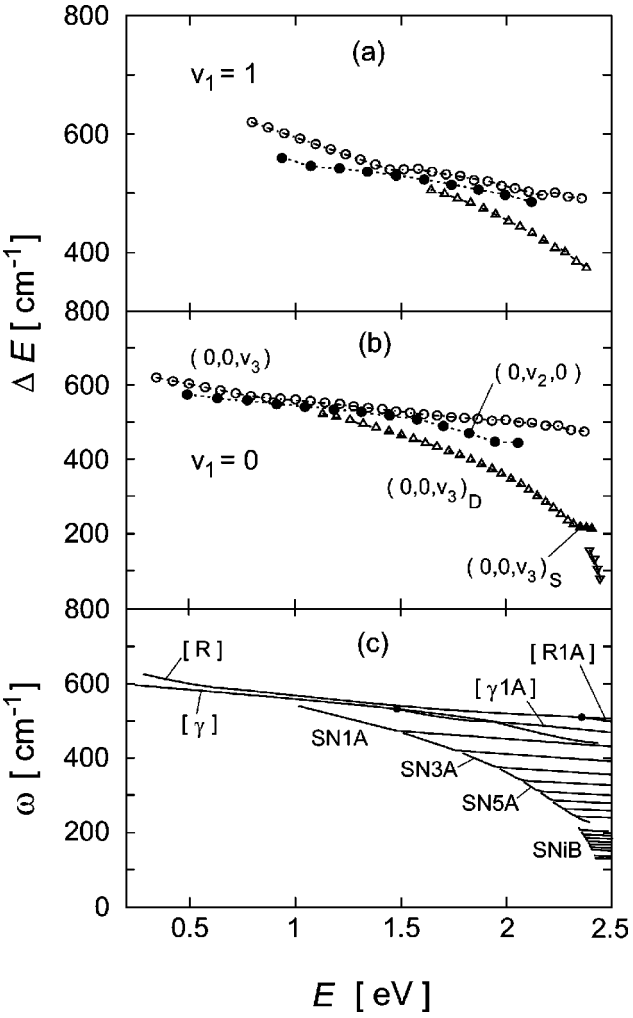

FIG. 2. (a) Energy differences between neighboring states of the pure progressions $(1,0,v_3)$ (filled circles), $(1,v_2,0)$ (open circles), and $(1,0,v_3)_D$ (open triangles) as functions of energy. The transition frequencies of the bending progression are divided by two. (b) The same as in (a), but for $v_1=0$. The filled triangles are for the S states. (c) Frequencies of the classical periodic orbits belonging to various families as indicated. The frequencies of the $[\gamma]$-type POs are divided by two, whereas the frequencies of the [R1A] family are multiplied by two. The classical frequencies are shifted by 0.23 eV, the zero-point energy of the v_1 mode, to higher energies. See the text for more details. Note, that the vertical scale in (a) is different from the vertical scales in (b) and (c).

POs. ''Pure'' bending states like (0,6,0) in Fig. 1 do not exist for $v_2\geqslant 11$. However, this new kind of bending states does not extend to much higher energies. (0,13,0) is the last member of the bending progression, as seen in Fig. 2(b). The change of the character of the bending states is also reflected by a slight change of the frequency around 1.7 eV in Fig. 2(b) corresponding to $v_2=11-12$. The same effect occurs also in HOCl, but at slightly higher polyads. Second, in a similar fashion, around $P=30$ the pure v_3 overtone states $(0,0,v_3)$, which at these high energies basically manifest excitation along the angular coordinate, also acquire excitation in the direction of R. An example, (0,0,30), is depicted in Fig. 3(e). Note the very different angular behavior of the states shown in Figs. 3(d) and 3(e). Again, this development of the quantum mechanical wave functions parallels the existence of a PD bifurcation of the classical periodic orbits that scar the $(0,0,v_3)$ states. A similar change has *not* been observed for HOCl.

B. Dissociation states

As thoroughly described for HOCl,[8] the regular pattern found for the lower polyads gradually changes as energy increases. States of the regular progressions in the middle of a polyad disappear and are replaced by states with a new kind of wave functions. This is already observed for $P=11$ and an example is seen in Fig. 1 for 1.193 eV, state $(0,0,12)_D$; this state would have the expected normal assignment (0,4,4), which, however, is difficult to recognize from

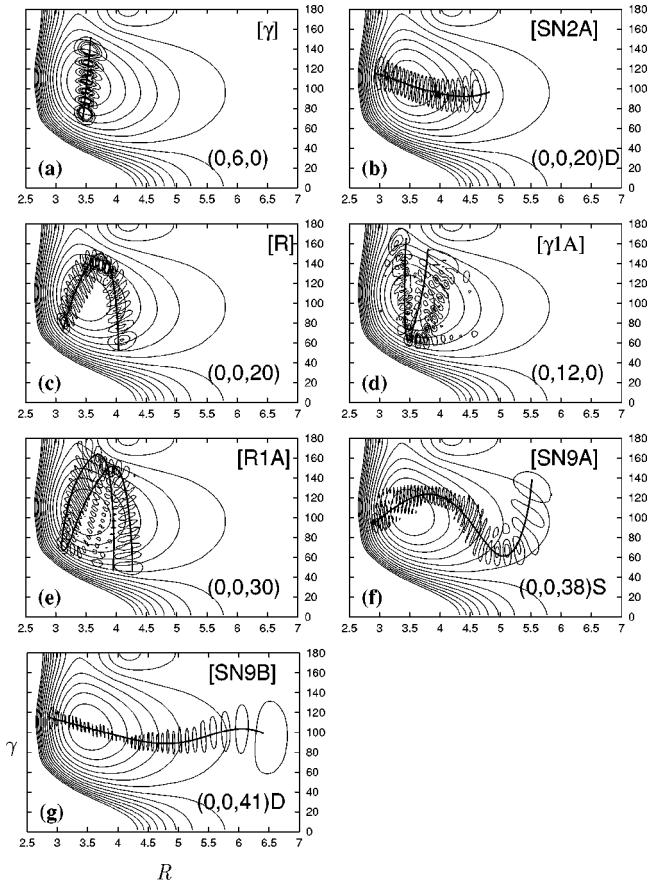

FIG. 3. Contour plots of wave functions for different types of quantum mechanical states as functions of R and γ. The HO coordinate r is integrated over. The solid lines represent corresponding classical periodic orbits calculated at comparable energies.

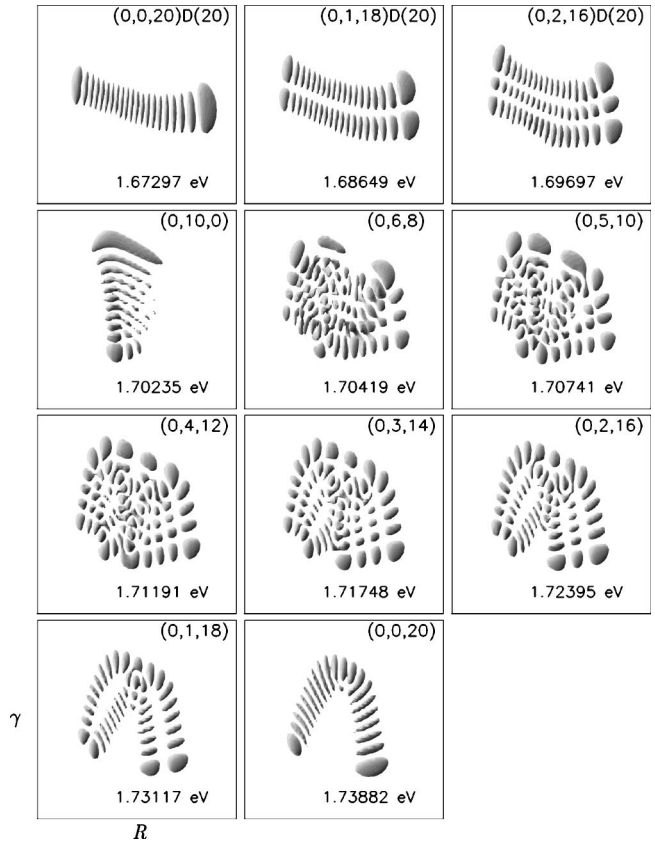

FIG. 4. Wave functions for polyad $P=20$. The γ axis ranges from 20° to 179° and the R axis ranges from $2.5a_0$ to $5a_0$. For more details see Fig. 1.

the level of the wave function contour used in Fig. 1. As energy increases the wave functions of the new states gradually become straighter and align along the dissociation coordinate R. Therefore, they have been termed dissociation (D) states in Ref. 8. Since the D states stretch along the dissociation path, they are more anharmonic than the $(0,v_2,0)$ and $(0,0,v_3)$ progressions [see Fig. 2(b)] and quickly drop below the regular states. For $P=20$ there are already three clear-cut D states below the (0,10,0) bending state (Fig. 4); three of the regular states are missing for this polyad: (0,9,2), (0,8,4), and (0,7,6). The number of states per polyad—$(P+1)/2$ for odd P and $(P+2)/2$ for even P—remains unchanged, however.

The appearance of the D states corresponds to a SN bifurcation in the classical phase space. However, while the birth of the analogous periodic classical trajectories happens at a particular sharp energy, the development of the D-state wave functions extends over a wider energy regime. As mentioned before, the third state from the bottom of polyad [0,12] in Fig. 1 can be either assigned as (0,4,4) according to the normal assignment at lower energies or, alternatively, as $(0,0,12)_{\mathrm{D}}$. The same holds true for the fifth and the sixth state of polyad [0,20] in Fig. 4. If there were not the bending state (0,10,0), the D states at the bottom of the polyad would gradually convert into the normal states at the top of the polyad. The smooth transformation from the bottom to the top is even more clearly seen in Fig. 5 for polyad [0,30], for which the corresponding bending state, (0,15,0), does not exist anymore, as discussed above. The states in the middle of the [0,30] polyad could be equally well assigned as D states or according to the normal assignment. Actually, the missing of the pure bending states at high excitation makes the very high polyads appear somehow simpler than the polyads at intermediate energies. Due to the better fulfillment of the resonance condition, the D states come to existence much earlier for HOBr than for HOCl and therefore there are many more such states for HOBr.

The progression of D states is terminated—or interrupted—at $P=35$, that is, the next states, $(0,0,36)_{\mathrm{D}}$ and $(0,0,37)_{\mathrm{D}}$, do not exist, at least not in the form found for the lower polyads. The wave functions for states $(0,0,34)_{\mathrm{D}}$ and $(0,0,35)_{\mathrm{D}}$ still look as expected, i.e., like $(0,0,30)_{\mathrm{D}}$ in Fig. 5, for example. However, the lowest states for polyads [0,36] and [0,37] depicted in the upper row of Fig. 6 look different. Their backbones have the structure of an inverted S and therefore we will call them ''S states'' in what follows. They are similar to the D states in that they also stretch along the dissociation path, certainly more so than the $(0,v_2,0)$ or the $(0,0,v_3)$ states. However, in contrast to the D states, the S states, more precisely the backbones of their wave functions, do not exceed the line $R\approx 6a_0$; instead of proceeding to the HO–Br asymptotic channel, they are deflected into the region of large angles.

With [0,38] the ''normal'' D states reappear and coexist with the S states in the same polyad, as illustrated in the

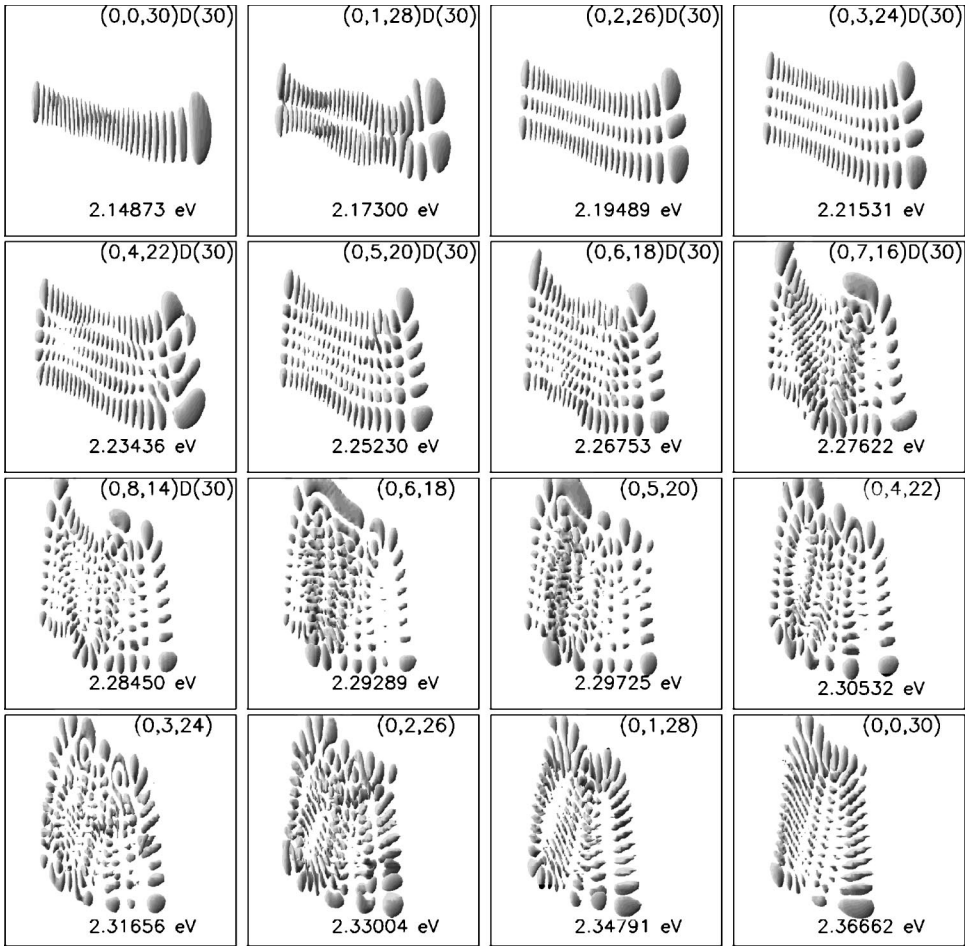

FIG. 5. Wave functions for polyad $P=30$. The (vertical) γ axis ranges from 20° to 179° and the (horizontal) R axis ranges from $2.5a_0$ to $5.5a_0$. For more details see Fig. 1.

three lowest rows of Fig. 6. For example, the states $(0,0,38)_D$ and $(0,0,38)_S$ are the lowest members of the [0,38] polyad. It is clearly seen that the S states do not extend along the dissociation path as far as the comparable D states. Because the S states ultimately avoid the dissociation path, they are less anharmonic than the D states [Fig. 2(b)]. As a consequence, the density of D states is higher than the density of S states. Both, the D and the S states persist up to the dissociation threshold and beyond; the clear nodal structure of the S states, however, becomes increasingly blurred with increasing energy [state $(0,0,39)_S$ in Fig. 6, for example]. A development somehow similar to the one described for HOBr has been found before for a two-dimensional model of HOCl, in which the HO coordinate was fixed.[23] The analysis of the classical phase space provides an explanation of the unusual behavior observed for HOBr.

In view of Fig. 2(b) we can roughly divide the $v_1=0$ spectrum into four regions according to the number of progressions. In the first region, extending to about 1.1 eV, there are only the bending and the HOBr stretching progressions, and the spectrum is simple. The second region extends from 1.1 eV to about 2.1 eV and is comparatively complicated; here, the two basic progressions are supplemented by the progression of D states, which rapidly move from the middle of the polyad to the lower end with increasing polyad quantum number. The D states continue the low-energy branch of the $(0,0,v_3)$ states to high energies. Actually, it are the D states that allow the system to dissociate. In the third region, ranging from about 2.1 to *ca.* 2.3 eV, the general appearance becomes simpler again due to the missing of the bending states. The $(0,0,v_3)$ states at the top of a polyade gradually mutate into the D states at the bottom. Finally, due to the appearance of the S states as well as the generally increasing mixing between states, the spectrum becomes more complex again at higher energies. This division into four energy regions is also supported by the classical phase space structure and the number of stable POs in the respective regions of the spectrum.

C. Polyad structure for $v_1 \neq 0$

The OH stretching mode is, for two reasons, to a large extent separated from the two degrees of freedom involved in the Fermi resonance. First, the potential coupling between r, on the one hand, and R and γ, on the other, is very weak.[24] Second, the fundamental frequency is considerably larger than the other two fundamental frequencies. As a result, the polyads for $v_1 \geqslant 1$ are qualitatively similar to those for $v_1=0$; they are merely shifted to higher energies by roughly the OH excitation energy [see Fig. 2(a) for $v_1=1$]. For example, the birth of the D states for $v_1=1$ takes place about 4000 cm^{-1} above the onset of the corresponding D states for $v_1=0$.

As already discussed by Peterson,[24] a 1:3 resonance be-

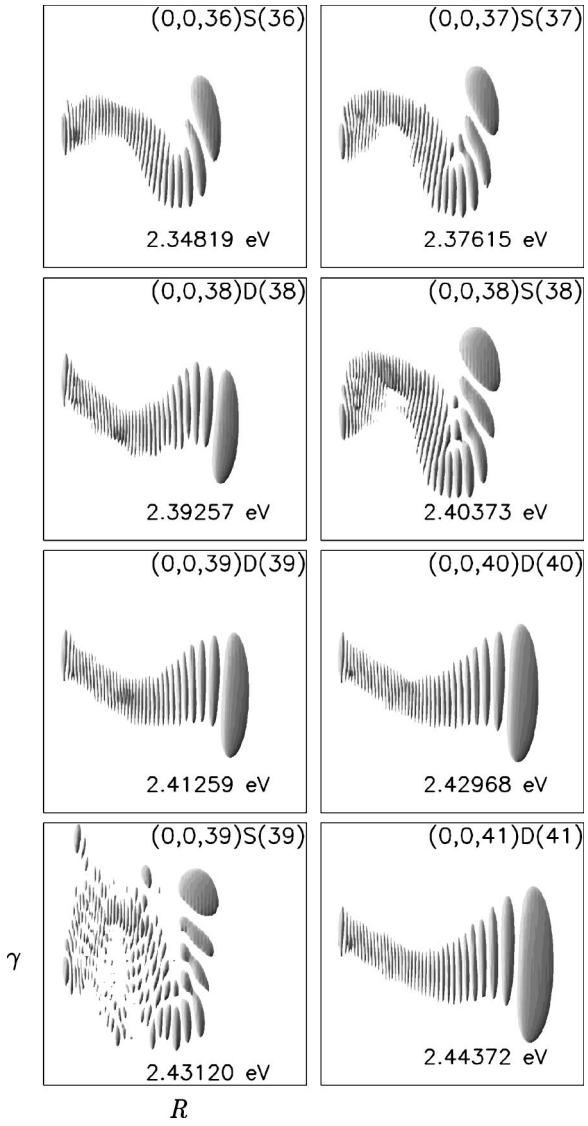

FIG. 6. Wave functions of a selection of S and D states in polyads [0,36] through [0,41]. The γ axis ranges from 20° to 179° and the R axis ranges from $2.5a_0$ to $7.5a_0$. For more details see Fig. 1.

tween the OH stretch and the bend affects the spectrum for $v_1 \geqslant 3$, i.e., states like $(v_1,0,0)$ and $(v_1-1,3,0)$ are mixed. This mixing becomes stronger and stronger with increasing v_1 since the separation between these two progressions becomes smaller with increasing energy. It results in many uncertain assignments at higher energies. In particular, the pure overtone states $(v_1,0,0)$ are more perturbed than the corresponding states in HOCl.

IV. ANALYSIS OF THE CLASSICAL PHASE SPACE

The correspondence between the morphology of quantum eigenfunctions and structures of the classical phase space has been studied extensively in the past.[1,2,12] The foundation of the phase space structure are periodic orbits (POs), stable as well as unstable ones.[9,33] By following the POs as they evolve with energy, one constructs a continuation/bifurcation (C/B) diagram.[11] In many applications, it has been demonstrated that the stable POs scar the quantum mechanical wave functions.[34] Examples of wave functions and corresponding POs for HOBr are depicted in Fig. 3. The finding of POs and their continuation in energy has been amply described in previous applications.[11,35,36]

The C/B diagram of HOBr, which is very similar to the one for HOCl,[8] is shown in Fig. 2(c). Here, we plot the frequency associated with each periodic orbit ($\omega = 2\pi/T$, where T is the period) as a function of the total energy of the system, E. This frequency, multiplied by $\hbar$, can be compared with the energy differences of adjacent overtone levels in the quantum mechanical study depicted in Fig. 2(b). All classical curves are shifted by 0.23 eV to higher energies, the quantum mechanical zero-point energy of the HO stretching mode. For a triatomic molecule, there are three principal families of POs, which, in correspondence to the three normal modes, are denoted as [r], [γ], and [R], respectively, because at low energies the POs basically describe motions along the three coordinate axes. The [r], [γ], and [R] families of POs correspond to the $(v_1,0,0)$, $(0,v_2,0)$, and $(0,0,v_3)$ progressions of the quantum mechanical states, as illustrated in Figs. 3(a) and 3(c) for [γ] and [R], respectively.

The [r] POs continue to exist up to very high energies, far above the threshold, and they are stable for the entire energy regime studied; they are not further discussed in what follows. The [γ] principal family of POs, in contrast, shows a PD bifurcation, [γ1A], at an energy of about 1.5 eV (the zero-point energy OH being included). Beyond the [γ1A] PD, the [γ] POs are singly unstable and at higher energies become even doubly unstable. In HOCl, the [γ] principal family of POs exhibited an early SN bifurcation because of a resonance with the r mode. This is not found for HOBr. The [γ1A] family, born at the PD bifurcation, is initially stable, but quickly becomes complex unstable. The POs of the [R] family are also stable up to very high energies. They turn to singly unstable at about 2.3 eV, giving birth to a new family of periodic orbits with double period, [R1A]. Similar to the [γ] principal family, there is no early SN bifurcation, as was found for HOCl. The [R1A] POs are initially stable, turn to complex unstable, and finally to doubly unstable. Examples of [γ], [γ1A], [R], and [R1A] POs are depicted in Figs. 3(a), 3(d), 3(c), and 3(e), respectively, together with corresponding quantum mechanical wave functions for similar energies. It is clear that the [γ1A] POs scar the high-overtone bending states with $11 \leqslant v_2 \leqslant 13$. Likeweise, the [R1A] POs scar the very high $(0,0,v_3)$ states. The effect of the period doubling is clear, when one compares [γ] with [γ1A] and [R] with [R1A].

POs that correspond to the D states in the quantum spectrum come into existence at a first saddle-node (SN) bifurcation,[37] SN1A, around 1 eV. The comparison with a D-state wave function for a comparable energy in Fig. 3(b) clearly demonstrates the correspondence. As energy increases, a resonance between R and r sets in, leading to a structural change of the SN1A POs and the change of the slope of the corresponding frequency curve.[8] However, the dissociation-type POs are continued in a second SN bifurcation, SN2A. We can see in Fig. 2 that this scenario is repeated as energy increases. All SN frequency curves exhibit the same qualitative pattern as the one for [R], that is, a short branch with a relatively large anharmonicity—which appears

to be the extrapolation of the low-energy segment of the [R] family—and a second branch for which the slope is very small, approximately the same slope as for the high-energy part of the [R] family.

The dissociation-type POs that scar the D states belong to the more anharmonic branches of the SNiA frequency curves and their general structure does not change much up to about SN7A. However, from the SN7A family onward these POs do change and acquire an ''S''-type form similar to the wave functions of the S states described in Sec. III B. Figure 3(f) shows an example for the SN9A family. Naturally, these are the POs that correspond to the S quantum states. The detailed analysis of the high-energy SNiA bifurcations clearly shows that the S-type POs belong to the families of SNiA POs. In this sense, one can consider the S states as the continuation of the lower-energy D states, despite the quite different anharmonicity.

Although a cascade of SN bifurcations similar to SN1A, SN2A, etc. has been found for other molecules (HOCl[8] and HCP,[38] for example), this is the first time to see that the less anharmonic segments of the curves actually influence three-dimensional quantum mechanical states. The early appearance of the D states in HOBr, as compared to HOCl, leaves more opportunity for these subtle classical effects to develop before the dissociation threshold is reached.

At the energy of 2.35 eV, a new series of SN bifurcations sets in, which are denoted as SN1B, SN2B, etc. in Fig. 2(c) (not all of them are shown). The projection of a representative PO in the (R,γ) plane is shown in Fig. 3(g); its energy lies on the more-anharmonic part of the last branch depicted in Fig. 2(c). It looks similar to the lower-energy SNiA POs, but extends far into the dissociation channel. It is this type of POs that carries the molecule toward the HO–Br dissociation channel. Their anharmonicity is higher than for the SNiA-type POs and the frequency quickly becomes smaller and smaller with increasing energy. This is in accord with the corresponding quantum mechanical states, that is, the high-energy branch of the D states [Fig. 2(b)]. Both, the quantum mechanical and the classical frequency curves suggest that the high-energy D states and the SNiB POs are the continuation of the low-energy D states and the low-energy SNiA POs, respectively. The present study as well as previous ones for other triatomic molecules, for which we have carried out similarly detailed analyses,[39] lead us to conclude that the appearance of a cascade of SN bifurcations, as the dissociation (or isomerization) limit is approached, is a common effect.

The classical PO examination explains most of the changes in the quantum mechanical spectrum. For example, the change of the bending states $(0,v_2,0)$ around $v_2=11$ is a consequence of the PD bifurcation of the $[\gamma]$ POs and the ''following'' of the quantum wave functions the $[\gamma 1A]$ POs. Shortly after the PD bifurcation the $[\gamma 1A]$ POs become unstable and, accordingly, the pure bending wave functions cease to exist. Likewise, the interruption of the D-state progression close to the threshold, the appearance of the S states, and the re-emerging of the D states parallels the cascades of SNiA and SNiB periodic orbits.

V. SEMICLASSICAL ANALYSIS

Additional insight into the dynamics of HOBr comes from the semiclassical analysis of a Fermi resonance model, which is simple enough to be integrable and therefore amenable to semiclassical studies, that is, one-dimensional quantization, but nevertheless reproduces the exact quantum spectrum remarkably well. Only the energy region close to threshold, i.e., region four in our classification in Sec. III is not described by the effective Hamiltonian model. Similar studies have recently been performed for HCP,[2,13,40] DCP,[4] and HOCl[7] (see also Ref. 1).

A. Resonance Hamiltonian model

As for HOCl, the Fermi resonance Hamiltonian for HOBr has the following nonvanishing matrix elements in the (direct product) harmonic oscillator basis,

$$\langle v_1,v_2,v_3|H|v_1,v_2,v_3\rangle=\sum_i \omega_i n_i+\sum_{i\leqslant j} x_{ij}n_i n_j + \sum_{i\leqslant j\leqslant k} y_{ijk}n_i n_j n_k+\cdots, \quad (1)$$

where $n_i=v_i+1/2$, and

$$\langle v_1,v_2,v_3|H|v_1,v_2-1,v_3+2\rangle = \sqrt{v_2(v_3+1)(v_3+2)}\left(k+\sum_i k_i n_i+\sum_{i\leqslant j} k_{ij}n_i n_j+\cdots\right), \quad (2)$$

with $n_1=v_1+1/2$, $n_2=v_2$, and $n_3=v_3+3/2$. The indices 1–3 have the same meaning as before in the quantum study. In this model the OH stretch quantum number and the polyad number are good quantum numbers for the Fermi resonance Hamiltonian, whereas they are only approximate quantum numbers in an exact treatment.

The parameters ω_i, x_{ij}, y_{ijk},..., k, k_i,..., of Eqs. (1) and (2) were adjusted so that the eigenvalues and wave functions of the Fermi resonance Hamiltonian accurately reproduce those of the exact Hamiltonian. The first 592 bound states of HOBr (out of the 708 calculated ones) were taken into account in the fit, that is, all states up to more than 95% of the dissociation threshold. These states include up to 30 quanta in the OBr stretching degree of freedom. With a set of 28 parameters,[32] the exact energies of these 592 states are reproduced with a root mean square error of 7.66 cm^{-1} and a maximum error of 41.9 cm^{-1}. The largest errors are systematically observed for states with large values of both v_1 and v_2, which indicates that some small—but systematic—coupling between the OH stretch and the bend is active in the real Hamiltonian, which, however, is not taken into account by the Fermi resonance Hamiltonian. Except for the apparent symmetry in the q_2 coordinate, caused by the approximate linear relationship between Jacobi and normal coordinates, the semiclassical wave functions compare well with the exact ones. The wave functions for the 16 states belonging to polyad $[v_1,P]=[0,30]$ can be obtained electronically[32] and compared with the exact wave functions for the same polyad in Fig. 5.

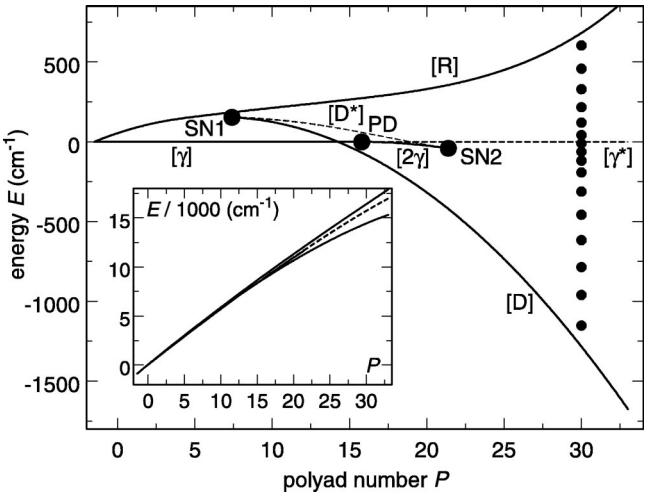

FIG. 7. Energies of the periodic orbits, obtained from the effective Hamiltonian, as functions of the polyad number P for $v_1=0$. In the small insert, the energies are plotted relative to the quantum mechanical ground state. In the main figure, the energies are plotted relative to the energy of the pure bending periodic orbit, $[\gamma]$. The heavy dots marked SN1, SN2, and PD indicate the two saddle-node and the period-doubling bifurcations, respectively. Stable periodic orbits are indicated by the solid lines, while unstable periodic orbits are represented by the dashed curves. The vertically arranged small dots for $P=30$ indicate the quantum mechanical energy levels. See the text for more details.

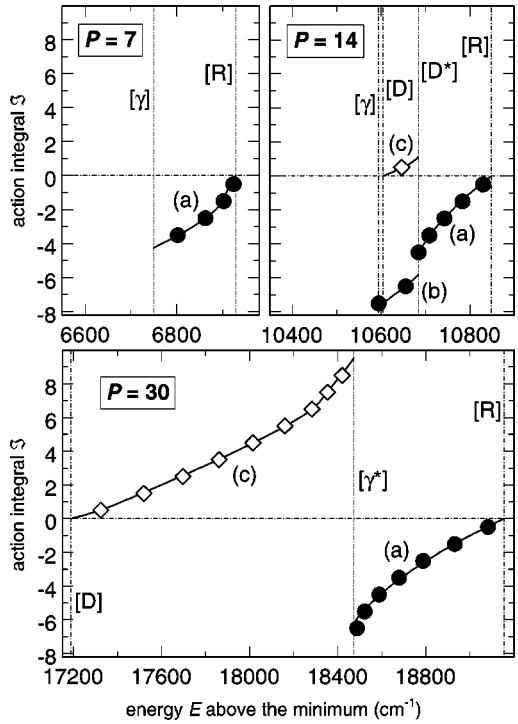

FIG. 8. The action integral $\mathcal{I}$ as a function of the absolute energy E for polyads $[v_1,P]=[0,7]$, $[0,14]$, and $[0,30]$. The vertical lines indicate the energies of the various periodic orbits. The quantum mechanical states belonging to the normal and the new progression are indicated by the filled circles and the open diamonds, respectively. Note, that the horizontal energy scale for polyads $P=7$ and $P=14$ is expanded twice compared to $P=30$.

B. Periodic orbits and one-dimensional quantization

As in the analysis of the exact classical phase space, Sec. IV, the POs in the subspace (p_2,p_3,q_2,q_3) of the dimensionless coordinates, coupled by the Fermi resonance, are the key for understanding the quantum spectrum of the resonance Hamiltonian. Once the classical constants of motion associated with the good quantum numbers v_1 and P have been quantized according to the Einstein–Brillouin–Keller (EBK) quantization rules [see Eq. (10) of Ref. 7], these POs are very easily found as the fixed points of the one-dimensional classical counterpart of the Fermi resonance Hamiltonian.[1] In comparison to the exact classical approach, the semiclassical analysis has the fundamental advantage that the POs are determined for a particular polyad $[v_1,P]$ instead of just energy. Consequently, in a semiclassical continuation/bifurcation diagram, the energies of the POs are plotted as a function of P for a particular value of v_1. Such a semiclassical C/B diagram is shown in Fig. 7 for $v_1=0$. Because of the resonance condition $\omega_2\simeq 2\omega_3$, the energies of the POs associated with a particular polyad $[v_1,P]$ are almost degenerate (see the small insert in Fig. 7). For a clearer representation, the energies of the POs are therefore plotted with respect to the energy of the pure bend PO in the main part of Fig. 7. It is emphasized that the energies of the quantum states belonging to a given polyad always lie between the energies of the two outermost stable POs. This is illustrated in Fig. 7, where the energies of the 16 states belonging to polyad $[v_1,P]=[0,30]$ appear as a stack of filled dots.

The C/B diagram in Fig. 7 is different from the one depicted in Fig. 2(c) in that it shows the real energies of the POs rather than frequencies. Nevertheless, the generic structure is very similar, except for very high polyads. For small values of P one finds two stable POs, $[\gamma]$ and [R], which correspond to motion along the HOBr bend (q_2) and the OBr stretch (q_3) coordinate, respectively. Periodic orbits that describe motion along the dissociation coordinate q_3 and that correspond to the D states are born at the first SN bifurcation, SN1, at $P=7.4$ corresponding to $E=4360\,\mathrm{cm}^{-1}$ above the quantum mechanical ground state; the families of stable and unstable POs are termed [D] and [D*], respectively. The [D] PO becomes the lower limit of the accessible phase space around $P\approx 14$ and eventually it scars the states located at the bottom of the polyads. The net result of the migration of the [D] PO toward the low-energy end of the polyad and the deformation of the [R] PO is that, starting with $P=15$, the states with a predominant bend character lie at the top of the polyad while those with predominant stretch character have dropped to the bottom of the polyad (see Figs. 4 and 5).

For the semiclassical quantization the plot of the action integral $\mathcal{I}$ as a function of energy E is important.[1] Each quantum state is associated, through the EBK quantization rules, to a trajectory with a half-integer value of $\mathcal{I}$. Examples for three different polyads are depicted in Fig. 8. For low values of P, for example $P=7$, there is only a single branch, that is denoted by (a). The quantizing trajectories—and therefore the quantum states—are indicated by the black dots in Fig. 8.

At the SN1 bifurcation the branch (a) of the action integral splits into two branches: (a) and (b), and a third one, (c), appears, which extends between the energies of the [D] and the [D*] POs (see $P=14$ in Fig. 8). The two branches (a) and (b) still support quantum states belonging to the normal

progression characteristic for the low-energy region. However, one state of this progression disappears each time the energy gap between the two branches becomes sufficiently wide to encompass an additional half-integer value of $\mathscr{T}$. Each state disappearing from the normal progression is replaced by a member of the new progression of the dissociation states D. The D states are supported by branch (c) born at the SN1 bifurcation. One additional dissociation state appears in the quantum spectrum each time branch (c) widens sufficiently to encompass an additional half-integer value of $\mathscr{T}$.

As already discussed in the quantum mechanical part, the spectrum becomes simpler again around $P \approx 24$. Within the resonance Hamiltonian model the reason for this phenomenon is that—as the consequence of two additional bifurcations—the bending PO, which is located between [R] and [D], is destroyed. More precisely, for $v_1 = 0$, HOBr undergoes a PD bifurcation at $P = 15.8$, or $E = 8800\,\mathrm{cm}^{-1}$ above the quantum mechanical ground state. Here, the pure bend PO $[\gamma]$ becomes unstable ($[\gamma^*]$) while the PO created at the PD bifurcation remains stable ($[2\gamma]$), respectively. However, the PD bifurcation is very rapidly followed, at $P = 21.4$, or $E = 11\,600\,\mathrm{cm}^{-1}$, by a second SN bifurcation, SN2, where the unstable PO [D*] and the stable PO $[2\gamma]$ are simultaneously destroyed. For polyads with $P \geqslant 22$, the accessible classical phase space therefore extends between the [D] and the [R] stable POs, with the unstable $[\gamma^*]$ PO playing the role of the separatrix between the two types of motion. Moreover, branch (b) disappears in the action integral $\mathscr{T}(E)$ at the bifurcation SN2. Consequently, for $P \geqslant 22$, all the members of the new progression are located below $[\gamma^*]$ on the (c) branch, while all the surviving members of the normal progression are located above $[\gamma^*]$ on the (a) branch (see the semiclassical wave functions for $P = 30$, Ref. 32). The facts that, first, only two stable POs remain for scaring wave functions and, second, members of the normal and the new progressions can no longer be interwoven, explain why the high-energy polyads with $P \geqslant 22$ appear simpler than the polyads at intermediate energies.

Comparing the semiclassical results with the classical ones, the following observations are made: (i) There is agreement for the saddle node bifurcations (denoted by SN1A in the classical analysis and by SN1 in the semiclassical treatment) as well as for the energies of the PD bifurcations for the bending motion. (ii) The effective Hamiltonian reproduces only the first classical SN bifurcation, SN1A, and the principal high-slope branches of the successive SNiA bifurcations; the SNiAs with $i > 1$ are due to resonances between γ and r, which are not taken into account in the effective Hamiltonian. (iii) The SN2 bifurcation, which does not appear in the classical CB diagram, probably corresponds to the energy where the classical bend PO becomes doubly unstable. The R1A PD bifurcation in the classical treatment and the occurrence of the S states is not described by the semiclassical description; they occur at energies not taken into account in defining the effective Hamiltonian.

To conclude this section, we add that the polyads with $v_1 \geqslant 0$ behave like those with $v_1 = 0$, in the sense that the bifurcations take place at comparable values of P. More precisely, in the energy range investigated with the Fermi resonance Hamiltonian, the SN1 bifurcation occurs at $P = 7.4$ ($E = 4360\,\mathrm{cm}^{-1}$), $P = 8.4$ ($E = 8540\,\mathrm{cm}^{-1}$), $P = 8.7$ ($E = 12\,160\,\mathrm{cm}^{-1}$), and $P = 10.0$ ($E = 16\,173\,\mathrm{cm}^{-1}$) for $v_1 = 0$, 1, 2, and 3, respectively, while the PD bifurcation occurs at $P = 15.8$ ($E = 8800\,\mathrm{cm}^{-1}$) and $P = 20.7$ ($E = 14\,660\,\mathrm{cm}^{-1}$) for $v_1 = 0$ and 1, respectively.

VI. SUMMARY

(1) We have calculated all the bound states of HOBr using a recently calculated potential energy surface and the filter diagonalization technique. All wave functions have been visually inspected and assigned when possible. Many of the states, even close to the dissociation threshold, can be unambiguously assigned in terms of three quantum numbers. The results are qualitatively compared to HOCl.

(2) Like for HOCl, the spectrum for HOBr is dominated by a 1:2 anharmonic resonance that leads to an organization in terms of polyads $[v_1, P]$. At low energies, the bending states are at the bottom of the polyads, whereas the HO–Br stretching states are localized at the top. Due to the resonance the HO–Br stretching states acquire more and more bending character as energy increases.

(3) States, which advance along the HO–Br reaction path, called D states, come into existence at relatively low energies, much earlier than in HOCl. They are born in a saddle-node bifurcation. The D states are the continuation of the low-energy O–Br stretching states to high energies.

(4) Close to the threshold another kind of states appear, which also penetrate far into the dissociation channel; because of their shape, they are termed S states. In contrast to the D states, the S states are deflected away from the dissociation channel at large HO–Br distances and therefore exhibit a considerably smaller anharmonicity than the D states. They correspond to the less anharmonic branches of the high-energy SNiA bifurcations.

(5) The coexistence of the ''regular'' states characteristic for lower energies and the D states and the interleaving of these two types of states leads to a rather complicated pattern of the intrapolyad spectrum, just as for HOCl. However, the intrapolyad structure becomes simpler at high energies, because the bending states disappear. This is different from HOCl.

(6) The general evolution of the quantum mechanical states from low to high energies can be well explained in terms of the structure of the classical phase space, i.e., the various families of periodic orbits and the different types of saddle-node and period-doubling bifurcations. Additional insight is obtained by the semiclassical analysis of an effective Hamiltonian fitted to the quantum mechanical energies and wave functions.

ACKNOWLEDGMENTS

Two of the authors (T.A. and R.S.) gratefully acknowledge financial support by the Deutsche Forschungsgemeinschaft within the Sonderforschungsbereich 357 ''Molekulare Mechanismen Unimolekularer Reaktionen'' and by the

Fonds der Chemischen Industrie. They are indebted to Jan Hauschildt and Jan Weiß for their help with the quantum mechanical calculations and the assignment.

[1] M. Joyeux, S. C. Farantos, and R. Schinke, J. Phys. Chem. A **106**, 5407 (2002).
[2] H. Ishikawa, R. W. Field, S. C. Farantos, M. Joyeux, J. Koput, C. Beck, and R. Schinke, Annu. Rev. Phys. Chem. **50**, 443 (1999).
[3] C. Beck, R. Schinke, and J. Koput, J. Chem. Phys. **112**, 8446 (2000).
[4] J. Bredenbeck, C. Beck, R. Schinke, S. Stamatiadis, S. C. Farantos, and M. Joyeux, J. Chem. Phys. **112**, 8855 (2000).
[5] H.-M. Keller, H. Flöthmann, A. J. Dobbyn, R. Schinke, H.-J. Werner, C. Bauer, and P. Rosmus, J. Chem. Phys. **105**, 4983 (1996).
[6] H.-M. Keller, T. Schröder, M. Stumpf, C. Stöck, F. Temps, R. Schinke, H.-J. Werner, C. Bauer, and P. Rosmus, J. Chem. Phys. **106**, 5359 (1997).
[7] R. Jost, M. Joyeux, S. Skokov, and J. M. Bowman, J. Chem. Phys. **111**, 6807 (1999).
[8] J. Weiß, J. Hauschildt, S. Yu. Grebenshchikov, R. Düren, R. Schinke, J. Koput, S. Stamatiadis, and S. C. Farantos, J. Chem. Phys. **112**, 77 (2000).
[9] M. C. Gutzwiller, *Chaos in Classical and Quantum Mechanics* (Springer-Verlag, New York, 1990).
[10] H. S. Taylor, in *Molecular Dynamics and Spectroscopy by Stimulated Emission Pumping*, edited by H.-L. Dai and R. W. Field (World Scientific, Singapore, 1995).
[11] S. C. Farantos, Int. Rev. Phys. Chem. **15**, 345 (1996).
[12] M. E. Kellman, in Ref. 10.
[13] M. Joyeux, D. Sugny, V. Tyng, M. E. Kellman, H. Ishikawa, R. W. Field, C. Beck, and R. Schinke, J. Chem. Phys. **112**, 4162 (2000).
[14] M. P. Jacobson, C. Jung, H. S. Taylor, and R. W. Field, J. Chem. Phys. **111**, 600 (1999).
[15] C. Jung, H. S. Taylor, and M. P. Jacobson, J. Phys. Chem. A **105**, 681 (2001).
[16] R. Schinke, C. Beck, S. Yu. Grebenshchikov, and H.-M. Keller, Ber. Bunsenges. Phys. Chem. **102**, 593 (1998).
[17] J. M. Bowman, J. Phys. Chem. A **102**, 3006 (1998).
[18] J. Hauschildt, J. Weiß, C. Beck, S. Yu. Grebenshchikov, R. Düren, R. Schinke, and J. Koput, Chem. Phys. Lett. **300**, 569 (1999).
[19] S. Skokov and J. M. Bowman, J. Chem. Phys. **110**, 9789 (1999).
[20] S. Skokov, K. A. Peterson, and J. M. Bowman, J. Chem. Phys. **109**, 2662 (1998).
[21] S. Skokov, K. A. Peterson, and J. M. Bowman, Chem. Phys. Lett. **312**, 494 (1999).
[22] K. A. Peterson, S. Skokov, and J. M. Bowman, J. Chem. Phys. **111**, 7446 (1999).
[23] M. Joyeux, D. Sugny, M. Lombardi, R. Jost, R. Schinke, S. Skokov, and J. M. Bowman, J. Chem. Phys. **113**, 9610 (2000).
[24] K. A. Peterson, J. Chem. Phys. **113**, 4598 (2000).
[25] M. R. Wall and D. Neuhauser, J. Chem. Phys. **102**, 8011 (1995).
[26] T. P. Grozdanov, V. A. Mandelshtam, and H. S. Taylor, J. Chem. Phys. **103**, 7990 (1995).
[27] V. A. Mandelshtam and H. S. Taylor, J. Chem. Phys. **102**, 7390 (1995).
[28] J. C. Light and T. Carrington, Adv. Chem. Phys. **114**, 263 (2000).
[29] J. Echave and D. C. Clary, Chem. Phys. Lett. **190**, 225 (1992).
[30] Z. Bačić and J. C. Light, J. Chem. Phys. **85**, 4594 (1986).
[31] M. R. Wedlock, R. Jost, and T. R. Rizzo, J. Chem. Phys. **107**, 10344 (1997).
[32] See EPAPS Document No. E-JCPSA6-118-012321 for a list of the energies and assignments of the bound states of HOBr, the parameters of the resonance Hamiltonian, and the semiclassical wave functions for polyad [0,30]. A direct link to this document may be found in the online article's HTML reference section. The document may also be reached via the EPAPS homepage (http://www.aip.org/pubservs/epaps.html) or from ftp.aip.org in the directory /epaps/. See the EPAPS homepage for more information.
[33] P. Gaspard, D. Alonso, and I. Burghardt, Adv. Chem. Phys., 105 (1995).
[34] E. J. Heller and S. Tomsovic, Phys. Today **46**, 38 (1993).
[35] S. C. Farantos, Laser Chem. **13**, 87 (1993).
[36] M. N. Vrahatis, A. E. Perdiou, V. S. Kalantonis, E. A. Perdios, K. Papadakis, R. Prosmiti, and S. C. Farantos, Comput. Phys. Commun. **138**, 53 (2001).
[37] M. Golubistsky and D. G. Schaeffer, *Singularities and Groups in Bifurcation Theory* (Springer-Verlag, New York, 1985), Vol. I.
[38] C. Beck, H.-M. Keller, S. Yu. Grebenshchikov, R. Schinke, S. C. Farantos, K. Yamashita, and K. Morokuma, J. Chem. Phys. **107**, 9818 (1997).
[39] M. Founargiotakis, S. C. Farantos, H. Skokos, and G. Contopoulos, Chem. Phys. Lett. **277**, 456 (1997).
[40] M. Joyeux, S. Yu. Grebenshchikov, and R. Schinke, J. Chem. Phys. **109**, 8342 (1998).